



Article

Role of *Staphylococcus aureus*'s Buoyant Density in the Development of Biofilm Associated Antibiotic Susceptibility

Sarah Kispert ^{1,†}, Madison Liguori ^{1,†}, Cody Velikaneye ¹, Chong Qiu ¹ , Shue Wang ¹, Nan Zhang ² and Huan Gu ^{1,*}

¹ Department of Chemistry and Chemical Engineering & Biomedical Engineering, Tagliatela College of Engineering, University of New Haven, West Haven, CT 06516, USA

² Key Laboratory of Targeting Therapy and Diagnosis for Critical Diseases of Henan Province, Department of Pharmaceutics, School of Pharmaceutical Sciences, Zhengzhou University, Zhengzhou 450001, China

* Correspondence: hgu@newhaven.edu; Tel.: +86-203-932-7000

† These authors contributed equally to this work.

Abstract: Biofilms are clusters of microorganisms that form at various interfaces, including those between air and liquid or liquid and solid. Due to their roles in enhancing wastewater treatment processes, and their unfortunate propensity to cause persistent human infections through lowering antibiotic susceptibility, understanding and managing bacterial biofilms is of paramount importance. A pivotal stage in biofilm development is the initial bacterial attachment to these interfaces. However, the determinants of bacterial cell choice in colonizing an interface first and heterogeneity in bacterial adhesion remain elusive. Our research has unveiled variations in the buoyant density of free-swimming *Staphylococcus aureus* cells, irrespective of their growth phase. Cells with a low cell buoyant density, characterized by fewer cell contents, exhibited lower susceptibility to antibiotic treatments (100 µg/mL vancomycin) and favored biofilm formation at air–liquid interfaces. In contrast, cells with higher cell buoyant density, which have richer cell contents, were more vulnerable to antibiotics and predominantly formed biofilms on liquid–solid interfaces when contained upright. Cells with low cell buoyant density were not able to revert to a more antibiotic sensitive and high cell buoyant density phenotype. In essence, *S. aureus* cells with higher cell buoyant density may be more inclined to adhere to upright substrates.

Keywords: *Staphylococcus aureus*; persisters; buoyant density; heterogeneity; antibiotic susceptibility; biofilm; density gradient centrifugation



Citation: Kispert, S.; Liguori, M.; Velikaneye, C.; Qiu, C.; Wang, S.; Zhang, N.; Gu, H. Role of *Staphylococcus aureus*'s Buoyant Density in the Development of Biofilm Associated Antibiotic Susceptibility. *Microorganisms* **2024**, *12*, 759. <https://doi.org/10.3390/microorganisms12040759>

Academic Editor: Alexis Bazire

Received: 12 March 2024

Revised: 5 April 2024

Accepted: 8 April 2024

Published: 9 April 2024



Copyright: © 2024 by the authors. Licensee MDPI, Basel, Switzerland. This article is an open access article distributed under the terms and conditions of the Creative Commons Attribution (CC BY) license (<https://creativecommons.org/licenses/by/4.0/>).

1. Introduction

Biofilms consist of bacteria that adhere to surfaces and are enveloped in a self-secreted extracellular polymeric substance (EPS) [1–3]. Their robust resistance to antimicrobial agents such as antibiotics (or low-level of antibiotic susceptibility) arises from the protective shield offered by the EPS and other mechanisms such as the presence of dormant cells, termed “persisters” [4–7]. This resistance has made biofilms hard to eradicate [4,5]. As per data from the Centers for Disease Control (CDC, 2007), bacterial biofilms were linked to nearly 1.7 million hospital-related infections, translating to medical expenses of USD 11 billion [8]. The annual economic burden of infections related to biofilms in the US is approximately USD 94 billion, contributing to over half a million fatalities in the United States [9]. Given their profound impact, biofilm research and control have attracted extensive attention for the last thirty years.

The process of biofilm formation is known to include four major steps that are initial attachment, microcolony formation, maturation, and dispersion [10]. The initiation of biofilm formation is marked by bacterial attachment to solid substrates, like medical implant tissues [11]. Once bacteria get close to a substrate, they can achieve initial attachment via

extracellular structures such as flagella, pili, or adhesin proteins [11,12]. However, it is still ambiguous how free moving (or planktonic) bacteria approach substrates and what factors decide if a bacterium can get close to substrates, spurring the focus of this study. Insights from this study endeavor aim to enrich the formulation of potent strategies for biofilm prevention and eradication.

Bacterial buoyant density indicates a bacterial cell's propensity to float or settle within a fluid medium like a growth solution [13–15]. When comparing planktonic cells of varying buoyant densities, those with a higher buoyant density tend to settle more rapidly due to gravitational forces. Notably, in 1984, Kubitschek et al. reported variations in the buoyant density of *Escherichia coli* cells, exhibiting a consistent normal distribution irrespective of their growth pace [14]. Recent findings suggest a correlation between bacterial buoyant density, growth rate, and cell age [16–18]. However, this might not hold for persisters, a subset of bacteria known for having fewer cell organelles than their typical counterparts [19,20]. Intriguingly, persisters are consistently present in every bacterial population, independent of growth rates or population age.

To systematically investigate the buoyant density of a mixed population and obtain subpopulations with similar densities, we employed sucrose density gradient centrifugation in this study. Although sucrose density gradient centrifugation is commonly applied in separating nanoparticles [21,22], liposomes [23], membranes from tissues and cells [24], ribonucleic acids [25], or viruses [26,27], its incorporation in bacterial studies remains limited. Our research endeavors to harness this established technique to discern the influence of bacterial buoyant density on biofilm development and related antibiotic susceptibility. In this study, we selected *S. aureus* as the model microorganism due to its clinical importance and its resemblance to micron-scale biological entities. *S. aureus* is known as an opportunistic pathogen that can cause multidrug-resistant afflictions ranging from skin and respiratory infections [28,29] to food poisoning [30]. These spherical bacteria are devoid of external structures like flagella and lack motility [31]. Consequently, *S. aureus* cells can be viewed as static biological particles with minimal interactions, enabling an exclusive focus on buoyant density. Given the observed relationship between organelle count and buoyant density [20], we hypothesized that cells with elevated buoyant densities, due to their heightened metabolic activities, are more inclined to migrate towards and initially attach to upright substrates, driven by gravitational forces.

2. Results

2.1. For Any Isogenic *S. aureus* Population, There Was a Distribution of Cell Buoyant Density, Regardless of the Population's Age

To validate our hypothesis, we first conducted a gravity-driven sedimentation experiment using stationary phase *S. aureus* cells to quantitatively evaluate if there is a difference in the rate of sedimentation among the cells in an isogenic population. Based on Stokes' law [32], the sedimentation rate (v) is proportional to the buoyant density (B) of cells. Hence, the faster sedimentation rate represents higher buoyant density. To obtain an isogenic population, we used a single bacterial colony on an LB agar plate to inoculate bacterial growth. By carefully introducing a 15.50 h old isogenic *S. aureus* population at the top of 5.00 mL pre-chilled 0.85% NaCl solutions in 15.00 mL Falcon tubes and letting the cells settle for 15.00 min on ice, the difference in the rate of sedimentation was evaluated. The 0.85% NaCl solutions were used in this experiment to avoid osmotic pressure change and the effect of cell metabolic activities and division on the rate of sedimentation. The time of sedimentation was chosen as 15.00 min because it was the time taken for chemical diffusion to reach equilibrium [33]. By quantifying the sedimentation rates of cells in *S. aureus* in an isogenic population ($1.55 \pm 0.74 \times 10^9$ cells or 100.00%) using the drop-plate method and colony forming units (CFUs), we found that cells sink at different rates (Figure 1). It is worth noting that there were always $0.41 \pm 0.05\%$ or $6.37 \pm 0.79 \times 10^8$ cells that did not sediment in 15 min. Although the percentage was small, the absolute number of these cells was significant among the total population. Since the number of those cells was quantified

using CFUs, during which the number of viable cells was quantified, those cells that did not sediment were living cells. With the sedimentation rates in Figure 1, $51.17 \pm 6.24\%$ cells got the closest to the bottom surface of the 15.00 mL Falcon tube and were ready to make initial attachments. This portion of cells sediment faster, possibly due to the higher buoyant density.

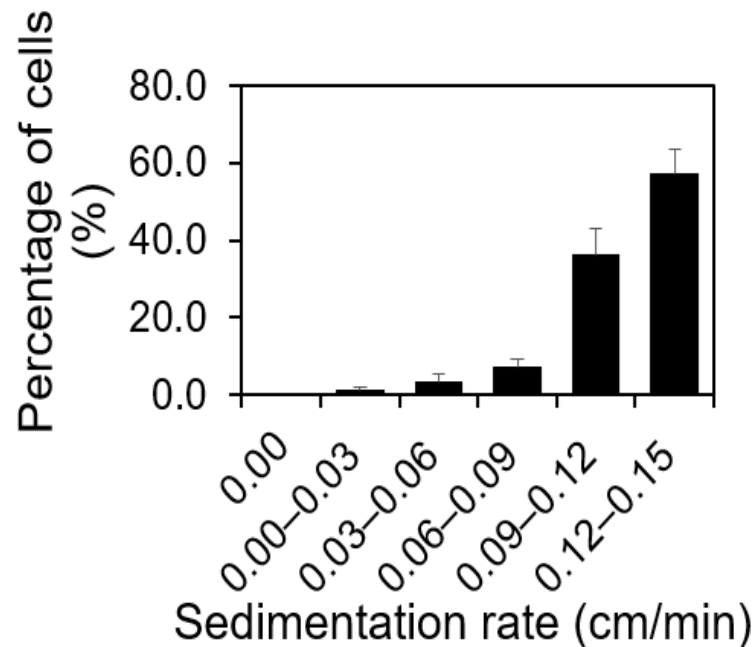


Figure 1. Gravity-driven sedimentation experiment. Percentage of *S. aureus* cells sedimenting at various speeds ($p = 0.00144 < 0.05$, t -test). In 15.00 mL Falcon tube with 5 mL 0.85% NaCl solution, cells sedimenting at 0.12–0.15 cm/min were the ones that were closest to the bottom of the upright 15.00 mL Falcon tube and ready for initial attachment after 15.00 min of gravity-driven sedimentation. This experiment was repeated biologically four times ($n = 4.00$). Standard errors are shown.

2.2. Correlating Sedimentation Rates with Cells' Buoyant Density Using Sucrose Density Gradient Centrifugation

The different sedimentation rates observed above indicate various buoyant density. To specifically characterize the buoyant density of cells in an isogenic *S. aureus* population, we used the sucrose gradient differential centrifugation. We prepared sucrose solutions with known densities (998.00, 1000.00, 1018.00, 1038.00, 1081.00, 1176.00, or 1230.00 kg/m³). By pulling an isogenic *S. aureus* population through a stack of sucrose solutions (or sucrose density gradient centrifugation), cells were separated based on their density. Cells with a density lower than that of a sucrose solution remained in the liquid layer sitting on top of the sucrose solution. Cells stopped in the sucrose solution had the same density (or $v = 0.00$ when $B = 0.00$ kg/m³ based on Stokes' law). Cells with density higher than that of the sucrose solution passed through the sucrose layers in response to the pulling force generated by centrifugation. They stopped in the layer of sucrose solution with the same density or precipitate at the bottom of the tube as a cell pellet if their density were larger than 1230.00. Using this method, we found that more than 86.32% of a 15.50 h old *S. aureus* population ($3.84 \pm 1.54 \times 10^8$ out of $4.45 \pm 3.39 \times 10^8$ ($p = 0.88$, t -test)) had a mass density higher than 1230.00 kg/m³ (Figure 2a). This could lead to a buoyant density (B) of 234.00 kg/m³, if those cells are suspended in solutions with a mass density like water (998.00 kg/m³), leading to sedimentation in response to gravity. It is worth noting that there is a heterogeneity in *S. aureus* cells' density and there is a subpopulation ($1.00 \pm 0.40 \times 10^{-3}\%$) with a mass density lower than that of water. Although the size of this subpopulation is small, the absolute cell number is significant ($4.34 \pm 1.66 \times 10^3$ among $4.45 \pm 3.39 \times 10^8$ cells ($p = 0.014 < 0.05$, t -test)).

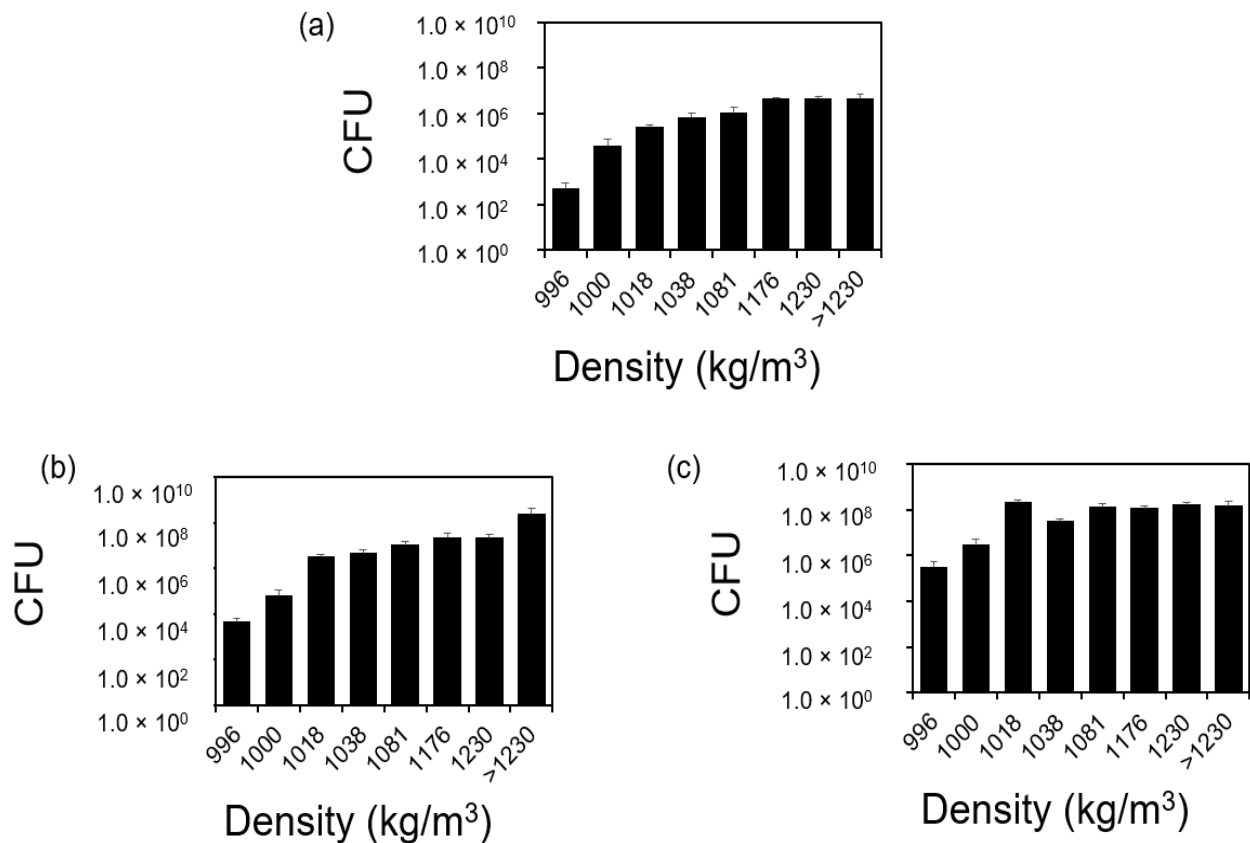


Figure 2. Sucrose gradient differential centrifugation. The distribution of the cells in 2.00 (a), 15.50 (b), and 18.00 (c) h old *S. aureus* populations. The total population (mix) was pulled through a stack of sucrose solutions with various mass densities (998.00, 1000.00, 1018.00, 1038.00, 1081.00, 1176.00, or 1230.00 kg/m^3) and separated based on mass density. The absolute number of cells was quantified using the drop plate method and CFUs [34]. Since the number of those cells was quantified using CFUs, during which the number of viable cells was quantified, those cells that did not sediment were living cells. Each separation was repeated five times biologically ($n = 5$). Standard errors are shown.

This heterogeneity in cell density is true regardless of growth age. However, the pattern of cell distribution at different densities varies according to growth age (Figure 2b,c). For instance, in an 18.00 h old *S. aureus* population, there were no *S. aureus* cells with densities higher than 1230.00 kg/m^3 and the percentage of *S. aureus* cells with densities lower than that of water increased to $0.06 \pm 0.05\%$ ($p = 0.21$, t -test) or $3.06 \pm 2.30 \times 10^5$ among $5.06 \pm 2.24 \times 10^8$ cells. We ruled out the effects of cell aggregation in this difference by fluorescently labeling cells before and after separation using Acridine Orange (AO) and microscopy. According to the fluorescence images (Supplementary Figure S1), we did not observe a significant amount of cell clusters before and after separation, suggesting that cell clusters did not contribute to the faster sedimentation. The investigation of the underlying mechanism is part of ongoing work. It is worth noting that the distribution of 18 h old *S. aureus* cells does not follow a normal distribution like *Escherichia coli* PAT 84 cells reported by Graetzer et al. [14] based on the probability plot in Minitab ($p < 0.05$, rejecting the null hypothesis that the distribution of our data is equal to a normal distribution). In a 2 h old exponential *S. aureus* population, 23.76% cells (or $3.16 \pm 3.00 \times 10^6$ out of $1.33 \pm 0.26 \times 10^7$ cells ($p = 0.65$, t -test)) had a mass density larger than 1230.00 kg/m^3 and the percentage of *S. aureus* cells with a density lower than that of water was $3.50 \pm 3.10 \times 10^{-3}\%$ (or $4.63 \pm 4.13 \times 10^2$ among $1.33 \pm 0.26 \times 10^7$ cells ($p = 0.0066 < 0.05$, t -test)). Since the number of those cells was quantified using CFUs, during which the number of viable cells was quantified, those cells that did not sediment were living cells. Although the percentage of cells with a density lower than that of water in the exponential phase *S. aureus* population

was higher than that in a 15.50 h old *S. aureus* population, the absolute number of cells remained low.

2.3. Cells with Higher Density Formed More Biofilms at the Liquid–Solid Interface Compared to Those with Lower Mass Density

Using sucrose density gradient centrifugation, we separated 15.50 h old *S. aureus* cells based on their mass density and compared their biofilm formation capabilities on the bottom surface of 96-well plates. The amount of biofilms formed by cells with different cell densities was quantified using crystal violet assay [35] (Figure 3). As shown in Figure 3, cells with higher mass density (1230.00 kg/m^3) formed more biofilms on the liquid–solid interface at the bottom surface of 96-well plates compared to cells with lower mass density (998.00 or 1000.00 kg/m^3), located at the air–liquid interface, which supports our hypothesis (t -test, $p = 0.028$ and $0.026 < 0.050$). They also formed slightly better biofilms compared to those formed by *S. aureus* cells without separation (t -test, $p = 0.21 > 0.05$). Since *S. aureus* cells without separation are mixtures of cells with both low and high densities, these results corroborate our hypothesis. Because we matched the sucrose background and cell numbers for inoculating biofilm growth, this difference in biofilm formation observed in Figure 3 was contingently due to the mass density of *S. aureus* cells.

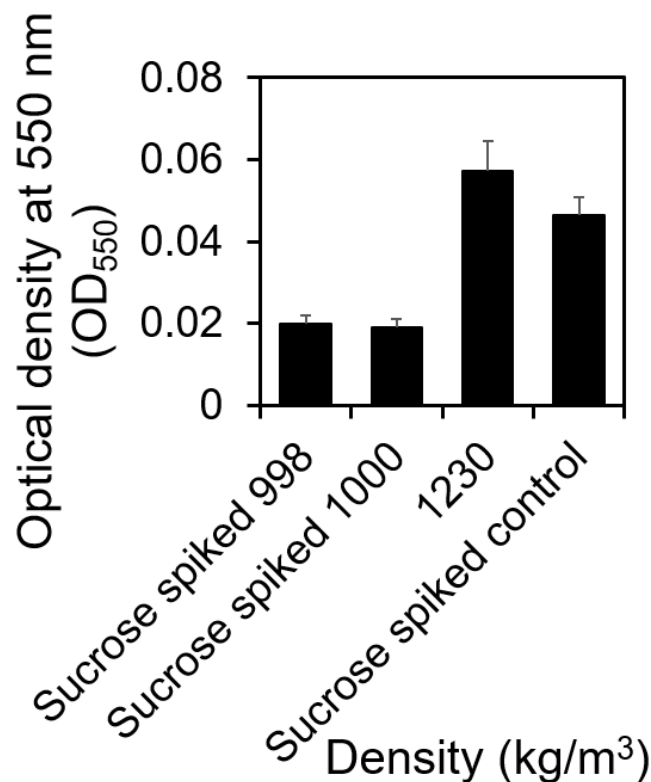


Figure 3. Biofilms that were formed by cells with different densities. Signals from biofilms formed by cells with low-level mass densities (998.00 and 1000.00 kg/m^3) and high-level mass density (1230.00 kg/m^3) after 48 h of incubation. The biofilms formed by the mixture of cells with varying densities before separation were used as controls. The biofilm formation was repeated four times biologically ($n = 4$). Standard errors are shown.

2.4. Cells with Higher Density Revived Faster from Nutrient Deprivation Than Those with Lower Density When Nutrients Were Supplemented

To investigate the correlations between biofilm formation and cell density, we evaluated the growth rate of cells with low-level mass densities (998.00 and 1000.00 kg/m^3) and high-level mass density (1230.00 kg/m^3) after they were resuspended in solutions with abundant nutrients (Figure 4).

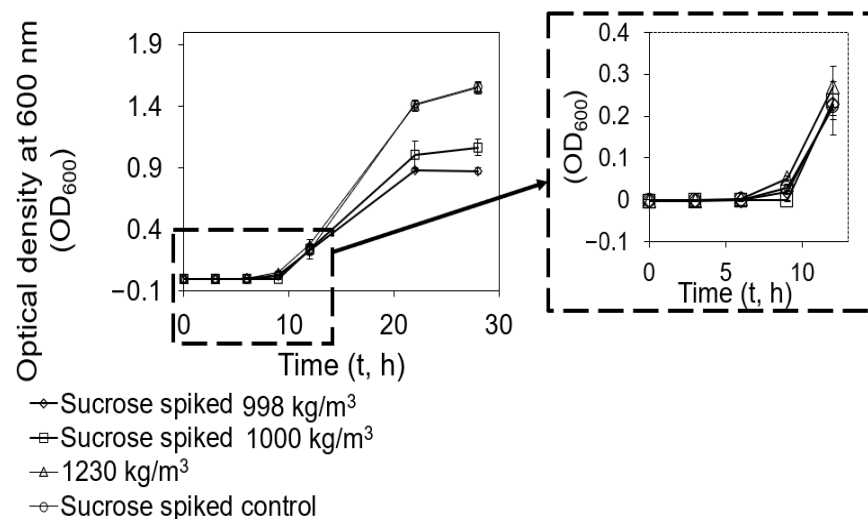


Figure 4. Cell growth rate. Cells with low-level mass densities (998.00 and 1000.00 kg/m³) and high-level mass density (1230.00 kg/m³) were isolated using sucrose density gradient centrifugation. Then, cells were resuspended into fresh LB with the same initial cell density. The optical cell density at 0.00, 3.00, 6.00, 9.00, 12.00, 22.00, and 28.00 h after inoculation was measured using a spectrophotometer. Each measurement was repeated biologically three times ($n = 3$). Standard errors are shown.

Based on the results, we found that *S. aureus* cells with high-level density (1230.00 kg/m³) started reproducing first at 6.00 h after inoculation (t -test, $p = 0.024, 0.033, \text{ or } 0.049 < 0.050$ compared to sucrose spiked cells with densities of 998.00 and 1000.00 kg/m³ or sucrose spiked mix, respectively), indicating that they are different. At 12.00 h after inoculation, the growth rate of cells with low-level densities caught up. However, at 22.00 h after inoculation, the growth rate of sucrose spiked cells with the density of 998.00 kg/m³ became significantly slower than cells with high-level density (t -test, $p = 0.0003$ and 0.0000 compared to cells with density of 1230.00 kg/m³ and sucrose spiked mix, respectively). At 28.00 h after inoculation, their growth rate was even slower than sucrose spiked cells with the density of 1000 kg/m³ (t -test, $p = 0.057$). Since we matched the sucrose concentration of cells with different densities after sucrose density gradient centrifugation, this difference in growth rate was contingently due to the heterogeneity in cell density. Since the number of those cells was quantified using CFUs, during which the number of viable cells was quantified, those cells that did not sediment were living cells.

2.5. Higher Percentage of Cells with Higher Buoyant Density Had DNA

To investigate the mechanism behind the heterogeneity in cell density, we first evaluated the correlation between the DNA and mass density (Figure 5). We used Acridine Orange (AO) to label the DNA [36] that emits green fluorescence when it binds to DNA. Using different illumination methods (brightfield vs. green fluorescence) to look at the cells in a 15.50 h *S. aureus* population after separation, we found that the distribution of cells with DNA labeled with green fluorescence followed a similar distribution to the cells that can be quantified using CFUs (DNA in Figure 5). However, the total number of cells identified using brightfield illumination was significantly greater than that quantified using CFUs, especially when the cell density was close to that of water (998.00 kg/m³). When the cells density was 998.00, 1000.00, 1018.00, and 1038.00 kg/m³, only 6.90, 0.62, 5.30, and 17.01% of the cells visualized by brightfield microscopy had their DNA labeled with AO (t -test, $p = 0.0006, 0.0541, 0.0283, \text{ and } 0.0100$, respectively). This percentage increased to 69.92, 53.99, and 77.38% when cell densities were 1081.00, 1176.00, and 1230.00 kg/m³, indicating that a higher percentage of cells with the density of 1230.00 kg/m³ had more DNA contents. We are confident that cells were not labeled due to the lack of DNA instead of the malfunction of the labeling. We observed a similar distribution of cells with and without fluorescent signals and the variations of fluorescent signals among cells with low

and high densities within three biological replicates. It is also well known that there is a small subpopulation of viable but non-culturable (VBNC) cells with low or no cell contents in every bacterial population [20].

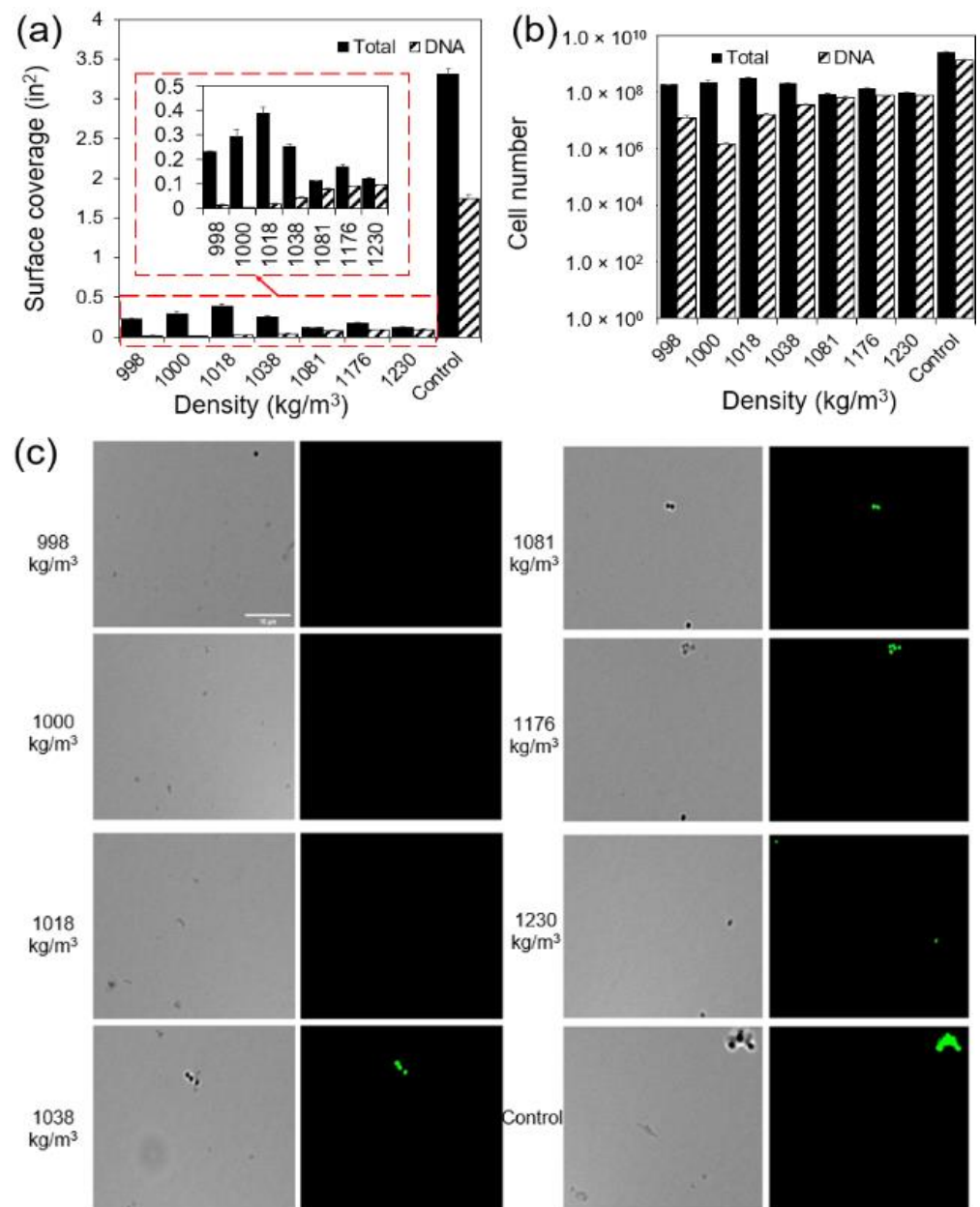


Figure 5. DNA content of cells with varying densities. Surface coverage (a) and the number (b) of cells with/without DNA labeled with green fluorescence. Surface coverage of total cells was characterized by analyzing the images taken by brightfield illumination. Surface coverage DNA was characterized by analyzing the images taken by green fluorescence (excitation: BP 470/40, FT 495 (HE), and BP 525/50 (HE)). Five random images were taken for each condition as technical repeats and each condition was repeated biologically three times ($n = 3$). Standard errors are shown. Image analysis comparison of brightfield and green fluorescence. (c) Zoomed in images of brightfield and green fluorescence channels for *S. aureus* cells with densities of 998.00, 1000.00, 1018.00, 1038.00, 1081.00, 1176.00, and 1230.00 kg/m³, respectively. The zoomed in images of mixed *S. aureus* cells before separation are included as controls (bar = 10 μm).

2.6. Cells with Higher Buoyant Density Were More Susceptible to Antibiotics

By directly visualizing the cells using a microscope, we found that cells with a higher buoyant density had more DNA content than those with lower buoyant density. To correlate this with the level of biofilm-related antibiotic susceptibility, we also quantified the level of antibiotic susceptibility of cells with various densities. As shown in Figure 6, cells with a density of 1230.00 kg/m³ were more susceptible to the one-hour treatment with 100.00 µg/mL vancomycin in 0.85% NaCl compared to cells with the densities of 998 and 1000 kg/m³ (*t*-test, *p* = 0.34). This difference in antibiotic susceptibility was contingently attributed to cells with different densities because we matched sucrose background before the antibiotic treatment.

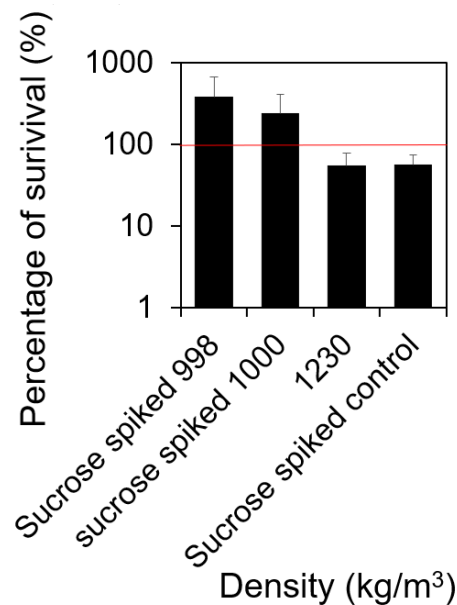


Figure 6. Susceptibility of cells with varying densities. The susceptibility of cells with the densities of 998.00, 1000.00, and 1230.00 kg/m³ were characterized by treating the cells separated using sucrose density gradient centrifugation with 100.00 µg/mL vancomycin for 1 h in 0.85% NaCl at 37 °C with shaking at 200 rpm. The number of cells surviving the treatment was quantified using the most probable number (MPN) assay [37]. The 100% of survival that represents no killing was highlighted using a red solid line. A percentage of survival higher than 100% could be due to cell division during antibiotic treatment. All experiments included in Figure 6 were repeated biologically five times (*n* = 5). Standard errors are shown.

3. Discussion

S. aureus biofilms rank among the primary culprits for infectious diseases, encompassing conditions from skin afflictions to septicemia [38–40]. The treatment of biofilm-driven infections is challenging due to the restricted permeability of antimicrobial agents through extracellular polymeric substances (EPSs), coupled with the prevalence of cells exhibiting reduced growth and metabolic rates, a result of stress responses in mature biofilms [4,5,41,42]. Despite the profound implications of biofilms, the complexity of their formation and emergent antibiotic resistance remains not fully deciphered [3,11,38,43]. Biofilm evolution encompasses four key phases: initial adherence, microcolony creation, maturation, and dispersion [33,44]. The initial attachment is critical to biofilm formation, but the exact factors dictating the shift from a planktonic state to a sessile one are yet to be entirely pinpointed. Notably, in contrast to bacteria *Escherichia coli* and *Pseudomonas aeruginosa*, *S. aureus* cells lack external structures, such as flagella or pili, to facilitate substrate engagement. The determinants governing the transition of *S. aureus* cells, particularly under forces like gravity and shear stress, remain veiled, thus sparking the interest behind this research.

Previously, it was well accepted that the density of bacterial cells, such as *S. aureus*, closely resembled that of water (998.00 kg/m^3), when determining biomass. However, this assumption might be flawed. If accurate, *S. aureus* cells would not gravitate towards a substrate's surface to initiate attachment, given the equilibrium between the cell's weight and the buoyant force within the solution. Our gravity-driven sedimentation experiment revealed differing sedimentation rates amongst *S. aureus* cells within an isogenic population (Figure 1). This disparity can primarily be linked to variations in the cells' buoyant densities, indicating a heterogeneity, even within an isogenic *S. aureus* population.

This heterogeneity in *S. aureus* cells' buoyant density was validated using sucrose density gradient centrifugation (Figure 2). This phenomenon was consistent across an isogenic *S. aureus* population at various growth stages, though the cell distribution pattern fluctuated based on the growth phase. For instance, in an exponential phase of the *S. aureus* population, around 30.23 ± 7.59 and $31.74 \pm 9.60\%$ cells exhibited mass densities of 1176.00 and 1230.00 kg/m^3 , respectively. The cell distribution during this phase did not follow a normal distribution based on the probability plot in Minitab ($p < 0.05$, rejecting the null hypothesis that the distribution of our data is equal to a normal distribution). Previously, Kubitschek et al. reported that exponential phase *E. coli* cells adhered to a tighter normal distribution [14]. The distinct sedimentation behavior of *S. aureus* and *E. coli* can be attributed to differences in their external structures, like flagella and pili. This pattern evolved as, in a 15.50 h old *S. aureus* sample, the percentages of cells exhibiting mass densities of 1176.00 and 1230.00 kg/m^3 dropped to 4.88 ± 2.58 and $4.68 \pm 2.03\%$ cells, respectively, and over 86.32% of cells demonstrated a density surpassing 1230.00 kg/m^3 . However, in an 18.00 h old sample, all *S. aureus* cells maintained a density at or below 1230.00 kg/m^3 , with the cell distribution deviating from the typical normal distribution based on the probability plot in Minitab, suggesting that the heterogeneity in cells' buoyant density varies dynamically.

Given the density of the LB broth was measured as 980.00 kg/m^3 , the observed variation in density can be translated to fluctuations in buoyant density when samples were introduced into the LB broth for biofilm formation (with buoyant densities of $B = -18.00, 20.00, 38.00, 58.00, 101.00, 196.00, \text{ or } 250.00 \text{ kg/m}^3$). Based on the correlation between sedimentation rate and buoyant density (Stokes' law), we hypothesized that cells possessing a higher buoyant density would gravitate towards the substrate and initiate attachment sooner. This conjecture was subsequently validated through our biofilm assay (Figure 3).

To investigate the mechanism behind the heterogeneity among cells in an isogenic *S. aureus* population, we analyzed the cellular content, particularly DNA, and growth rate of cells exhibiting different densities (Figures 4 and 5). A greater content within a specific volume signifies a higher cell density (Figure 5). Through microscopic examination of both the entire cell population and their DNA, we observed that subpopulations with densities of $998.00, 1000.00, 1018.00, \text{ and } 1038.00 \text{ kg/m}^3$ contained more cells than quantified via CFUs. Intriguingly, the majority of these cells lacked DNA signals. Previously, Kim et al. [20] showed that VBNC cells and persisters often contain reduced or negligible cellular content. This leads to the inference that cells exhibiting low buoyant densities might either be VBNC or persisters. Cells with a low buoyant density, due to their minimal content, displayed fewer DNA signals compared to their high-density counterparts, suggesting that those cells might be VBNC or persisters. This is corroborated by their slower growth rate after cell revival.

In evaluating the susceptibility of separated *S. aureus* subpopulations, we discerned that cells exhibiting a high buoyant density (1230.00 kg/m^3) were notably more responsive to $100 \text{ }\mu\text{g/mL}$ vancomycin than their lower buoyant density counterparts (998.00 and 1000.00 kg/m^3) (Figure 6). This mirrors Gu et al.'s prior findings [33], wherein initially attached *E. coli* cells displayed an enhanced susceptibility to antibiotics because of higher level metabolic activities. However, these initially attached cells rapidly lose their antibiotic susceptibility due to matrix secretion and subsequent microcolony development. This

transient heightened vulnerability in the initial phases may offer a unique opportunity for the effective elimination of *S. aureus* biofilms before they mature.

4. Conclusions

In this study, we found a heterogeneity in the buoyant density of isogenic *S. aureus* populations. This heterogeneity persists regardless of the population's age, but the cell distribution pattern evolves as the population ages, deviating from a narrow normal distribution. A higher buoyant density in *S. aureus* cells may be attributed to an increased cellular content, such as DNA. Intriguingly, cells demonstrating a higher buoyant density were more vulnerable to vancomycin, implying enhanced metabolic activity. It was supported by the 24 h LB broth culture, showing that *S. aureus* cells with higher buoyant density more effectively formed biofilms on the 96-well plate. Our findings corroborate the hypothesis that cells with higher buoyant density, due to their intensified metabolic activities, gravitate towards and initially adhere to upright substrates. This pronounced susceptibility to antibiotics among the early-attaching cells presents a promising avenue for proactive biofilm management and eradication.

5. Materials and Methods

5.1. Strains and Growth Media

S. aureus ALC2085 was first streaked onto lysogeny broth (LB) agar plates made of 10.00 g/L of NaCl, 10.00 g/L tryptone, 5.00 g/L yeast extract, and 15.00 g/L agar. This strain is sensitive to vancomycin with the minimal inhibitory concentration at 0.25 µg/mL [45]. The plates were incubated at 37 °C overnight. A colony was picked from the LB agar plate and used to inoculate fresh LB solution to grow *S. aureus* cells at 37 °C with shaking at 200 rpm. We chose LB solution for a better comparison with previously published results [46,47]. The day of the experiment, the optical density, OD₆₀₀, was determined by measuring the absorbance of the solution with a spectrophotometer, Spectrovis Plus (Vernier, Beaverton, OR, USA), then multiplying the value by a dilution factor of three. The OD₆₀₀ for the stationary and exponential phase cultures was required to be within the range of 1.50–2.00 and 0.10–0.50, respectively.

5.2. Density Gradient Centrifugation Separation

A series of sucrose solutions were prepared with diverse concentrations by dissolving sucrose (Sigma-Aldrich, St. Louis, MO, USA) into 0.85% NaCl solutions, resulting in distinct mass densities: 998.00 (0.85% NaCl solution), 1000.00 (5.00% wt/vol sucrose), 1018.00 kg/m³ (10.00% wt/vol sucrose), 1038.00 kg/m³ (20.00% wt/vol sucrose), 1081.00 kg/m³ (30.00% wt/vol sucrose), 1176.00 kg/m³ (40.00% wt/vol sucrose), and 1230.00 kg/m³ (50.00% wt/vol sucrose). All sucrose solutions and bacterial cultures were chilled on ice for no less than 15 min before sucrose gradient centrifugation. Then, 100.00 µL of chilled bacterial culture was slowly aspirated on top of each solution. The gradient solutions in microcentrifuge tubes were centrifuged at 4 °C and 170.00× *g* for the first 5 min, and then 1250.00× *g* for another 5 min as described previously [48]. After centrifugation, 100.00 µL from each layer of solutions was collected and placed in a 96-well plate.

Cell density in each layer of solutions was quantified using the drop plate method and colony forming units (CFUs) [34]. In detail, the 100.00 µL solutions from each layer were treated as the original samples and placed in the first column of the 96-well plate. These solutions were then diluted 10 times by transferring 20 µL of bacterial solution into 180.00 µL clean 0.85% NaCl for a dilution factor of 10. This step was repeated *n* times to reach a dilution factor of 10^{*n*} in column *n*. Upon mixing, 10.00 µL from each well was dropped onto an LB agar plate. The excessive 0.85% NaCl in each 10.00 µL droplet was air dried to fix the bacteria onto the LB agar plate. The dried LB agar plates were incubated at 37 °C overnight before the number of CFUs was counted.

5.3. Gravity-Driven Sedimentation

To corroborate the results obtained from density gradient centrifugation and prove that *S. aureus* populations are mixtures of cells with different buoyant density, we conducted a gravity-driven sedimentation. This assay was performed using test tubes filled with 0.85% NaCl solutions. Bacterial cultures, test tubes, and 0.85% NaCl solution were pre-chilled on ice for no less than 15.00 min. In each test tube, 5.00 mL of 0.85% NaCl solution was added. Then, 500.00 μ L of pre-chilled stationary phase *S. aureus* culture was carefully aspirated to the top of 5.00 mL cold 0.85% NaCl solutions in 15.00 mL Falcon tubes. After 15.00 min, the top 500.00 μ L was removed and the 0.85% NaCl solution was removed in 1.00 mL increments from the top. The time of sedimentation was chosen as 15.00 min because it was the time taken for chemical diffusion to reach equilibrium [33]. Cell number in each layer was quantified using drop plating and CFUs as described above.

5.4. Biofilm Inoculation

Cells from each layer separated using the density gradient centrifugation above and cells before separation (mix) were first spiked with sucrose to 50.00% to match the sucrose concentration of the layer with the mass density of 1230.00 kg/m³. Then, cells were diluted using 96-well plates by following the method of dilution described above for drop plating. The difference is that instead of using 0.85% NaCl solutions for dilution, we used LB solution. After dilution, the number of cells in each well was quantified by dropping 10.00 μ L cells onto LB agar plates and CFUs were counted. The 96-well plates were inoculated for 48 h to form biofilms. After 48 h biofilm formation, a crystal violet assay [35] was conducted. In detail, planktonic cells were dumped first, followed by three washes using 0.85% NaCl solutions. Then, we added 250.00 μ L 0.10% solution of crystal violet in water into each well. The 96-well plate was incubated at room temperature for 10.00–15.00 min. The dye was dumped, and the stained biofilms were washed three times using clean 0.85% NaCl solutions. The 96-well plate was dried overnight at room temperature by turning it upside down. The stained biofilms in each well were dissolved in 30.00% acetic acid in water. Absorbances were collected at 550 nm using a microplate reader (RayBiotech, Peachtree Corners, GA, USA) after 10.00–15.00 min incubation at room temperature. Guided by the CFUs, only the biofilms initiated with similar cell numbers were compared.

5.5. Antibiotic Susceptibility and Most Probable Number (MPN) Assay

Antibiotic susceptibility of *S. aureus* cells with different buoyant densities was evaluated by treating cells with 100.00 μ g/mL vancomycin in 0.85% NaCl solutions for 1.00 h at 37 °C while shaking at 200 rpm. The 0.85% NaCl solutions were used to avoid cell duplications during treatment. Cells from each layer separated using the density gradient centrifugation above and cells before separation (mix) were first spiked with sucrose to 50% to match the sucrose concentration of the layer with the mass density of 1230.00 kg/m³. Then, they were diluted in 0.85% NaCl solutions and LB solutions as described above for drop plating. Cells in each well were quantified using CFUs. Cells diluted in LB solutions were directly incubated overnight at 37 °C while shaking at 200 rpm to obtain the MPN [37] of the control. Cells diluted in 0.85% NaCl solutions were treated with 100.00 μ g/mL vancomycin for 1.00 h at 37 °C while shaking at 200 rpm. Treated samples were then transferred into a new 96-well plate, leaving a blank row of wells on each side of the well plate. Samples were diluted up to 10⁹ times with a dilution factor of 10 by transferring 20.00 μ L of bacterial solution into 180 μ L LB. The 96-well plates were then incubated at 37 °C while shaking at 200 rpm. The number of cells after treatment was determined by using the MPN method [37]. In detail, for each control or antibiotic treated sample, we treated the last dilution (e.g., 10ⁿ) that had change in OD₆₀₀ compared to the LB control that started with 1 cell. By doing this, we assumed that the original control or antibiotic treated sample had 10ⁿ cells, regardless of the changes in the original antibiotic treated samples or the 10¹ times dilution of the antibiotic treated samples. Due to the

continuous treatment by 100.00 and 10.00 µg/mL vancomycin, during the growth in the original antibiotic treated samples or the 10¹ times dilution of the antibiotic treated samples, there were no changes in the OD₆₀₀. However, with the increase in the times of dilution (e.g., 10ⁿ), the concentration of vancomycin decreased to 100/10ⁿ µg/mL that was too low to affect the growth of *S. aureus*. This was the reason we could calculate back how many cells stayed viable using MPN after antibiotic treatment. Since the viable cell number before treatment was also determined using MPN corroborated with CFUs, we are confident that antibiotic susceptibility can be quantified with the presence of antibiotics.

5.6. DNA Level Quantification Using Acridine Orange (AO) and Fluorescence Microscope

To quantify the DNA content of cells with different buoyant densities, we used Acridine Orange (AO), a nucleic-acid-selective fluorescent dye that can label DNA with green fluorescence (Ex. 500 nm and Em. 526 nm) [49]. In detail, we prepared 5.00 mg/mL Acridine Orange (Sigma-Aldrich, St. Louis, MO, USA) solution in DI water. Then, we diluted this working stock solution 10 times into the samples and incubated at room temperature for 3.00 min. After incubation, cells were imaged using a fluorescence microscope (Echo Revolve, BICO, Gothenburg, Sweden). Cells were illuminated with brightfield (black vs. white contrast for all bacteria) and a light source for exciting green fluorescence (for cells with DNA labeled with green fluorescence). Five images were taken at random spots for each condition. Each condition was repeated biologically three times.

ImageJ software (Image J 1.54d/Java 1.8.0_345 (64-bit)) was used for quantifying the surface coverage (in²) of total cells and cells with DNA labeled with green fluorescence. For black and white images taken using brightfield, the images were uploaded, and the threshold was set individually to achieve a clear contrast between the background and the bacteria. The bacteria should be displayed as small white particles shown clearly on a black background. For images of cells with green fluorescence, images were altered to be 16 bits first and then the threshold was set the same way as described prior for brightfield. By doing this, the background was removed and only bacteria can be seen in the images. The areas of surface coverage were calculated using the Analyze Particles function in ImageJ.

5.7. Statistics

For density gradient centrifugation, antibiotic susceptibility test, and biofilm formation at air–liquid and liquid–solid interfaces, each experiment was conducted with at least three biological replicates ($n \geq 3$) based on a power analysis ($n = 0.34 < 3$ when confidence $\alpha = 0.05$ and power 0.90) and studies reported previously ($n \geq 3$) [33,50]. Normal distribution was evaluated using a probability plot in Minitab. Statistical design of experiments, such as power analysis, factorial design, and complete randomization block design, was applied as appropriate. Collected data were analyzed using a *t*-test, *z*-test, correlation coefficient, analysis of variance (ANOVA), and Bonferroni method as appropriate. We defined statistical significance as a *p*-value less than or equal to 0.05.

Supplementary Materials: The following supporting information can be downloaded at: <https://www.mdpi.com/article/10.3390/microorganisms12040759/s1>, Figure S1: DNA content of cells for 18 h culture. Zoomed in images of brightfield and green fluorescence channels for *S. aureus* cells with the density of 1230.00 kg/m³. The zoomed in images of mixed *S. aureus* cells before separation are included as controls (bar = 10 µm).

Author Contributions: H.G. conceived the idea. H.G., M.L. and S.K. designed the experiments. M.L., S.K. and C.V. conducted the experiments. C.Q., S.W. and N.Z. participated in the manuscript preparation. All authors have read and agreed to the published version of the manuscript.

Funding: Huan Gu would like to acknowledge the funding support from the NASA CT Space Grant (80NSSC20M0129). Chong Qiu would like to acknowledge the funding support from the NSF Award #AGS-1847019. S. Wang would like to acknowledge the funding support from NSF CAREER (CMMI: 2143151).

Data Availability Statement: The original contributions presented in the study are included in the article/Supplementary Material, further inquiries can be directed to the corresponding author/s.

Conflicts of Interest: The authors declare no conflicts of interests.

References

1. Fulaz, S.; Vitale, S.; Quinn, L.; Casey, E. Nanoparticle–Biofilm Interactions: The Role of the EPS Matrix. *Trends Microbiol.* **2019**, *27*, 915–926. [[CrossRef](#)] [[PubMed](#)]
2. Desai, N.; Ardekani, A.M. Biofilms at interfaces: Microbial distribution in floating films. *Soft Matter.* **2020**, *16*, 1731–1750. [[CrossRef](#)] [[PubMed](#)]
3. Flemming, H.-C.; van Hullebusch, E.D.; Neu, T.R.; Nielsen, P.H.; Seviour, T.; Stoodley, P.; Wingender, J.; Wuertz, S. The biofilm matrix: Multitasking in a shared space. *Nat. Rev. Microbiol.* **2022**, *21*, 70–86. [[CrossRef](#)] [[PubMed](#)]
4. Lewis, K. Riddle of Biofilm Resistance. *Antimicrob. Agents* **2001**, *45*, 999–1007. [[CrossRef](#)] [[PubMed](#)]
5. Hall, C.W.; Mah, T.F. Molecular mechanisms of biofilm-based antibiotic resistance and tolerance in pathogenic bacteria. *FEMS Microbiol. Rev.* **2017**, *41*, 276–301. [[CrossRef](#)] [[PubMed](#)]
6. Manuse, S.; Shan, Y.; Canas-Duarte, S.J.; Bakshi, S.; Sun, W.S.; Mori, H.; Paulsson, J.; Lewis, K. Bacterial persisters are a stochastically formed subpopulation of low-energy cells. *PLoS Biol.* **2021**, *19*, e3001194. [[CrossRef](#)] [[PubMed](#)]
7. Zou, J.; Peng, B.; Qu, J.; Zheng, J. Are Bacterial Persisters Dormant Cells Only? *Front. Microbiol.* **2021**, *12*, 708580. [[CrossRef](#)]
8. Romling, U.; Kjelleberg, S.; Normark, S.; Nyman, L.; Uhlin, B.E.; Akerlund, B. Microbial biofilm formation: A need to act. *J. Intern. Med.* **2014**, *276*, 98–110. [[CrossRef](#)]
9. Wolcott, R.D.; Rhoads, D.D.; Bennett, M.E.; Wolcott, B.M.; Gogokhia, L.; Costerton, J.W.; Dowd, S.E. Chronic wounds and the medical biofilm paradigm. *J. Wound Care* **2010**, *19*, 45–53. [[CrossRef](#)]
10. Sharma, S.; Mohler, J.; Mahajan, S.D.; Schwartz, S.A.; Bruggemann, L.; Aalinkeel, R. Microbial Biofilm: A Review on Formation, Infection, Antibiotic Resistance, Control Measures, and Innovative Treatment. *Microorganisms* **2023**, *11*, 1614. [[CrossRef](#)]
11. Lee, S.W.; Phillips, K.S.; Gu, H.; Kazemzadeh-Narbat, M.; Ren, D. How microbes read the map: Effects of implant topography on bacterial adhesion and biofilm formation. *Biomaterials* **2021**, *268*, 120595. [[CrossRef](#)] [[PubMed](#)]
12. Howden, B.P.; Giulieri, S.G.; Wong Fok Lung, T.; Baines, S.L.; Sharkey, L.K.; Lee, J.Y.H.; Hachani, A.; Monk, I.R.; Stinear, T.P. *Staphylococcus aureus* host interactions and adaptation. *Nat. Rev. Microbiol.* **2023**, *21*, 380–395. [[CrossRef](#)] [[PubMed](#)]
13. Inoue, K.; Nishimura, M.; Nayak, B.B.; Kogure, K. Separation of marine bacteria according to buoyant density by use of the density-dependent cell sorting method. *Appl. Env. Microbiol.* **2007**, *73*, 1049–1053. [[CrossRef](#)] [[PubMed](#)]
14. Kubitschek, H.E.; Baldwin, W.W.; Graetzer, R. Buoyant density constancy during the cell cycle of *Escherichia coli*. *J. Bacteriol.* **1983**, *emph155*, 1027–1032. [[CrossRef](#)] [[PubMed](#)]
15. Baldwin, W.W.; Kubitschek, H.E. Buoyant density variation during the cell cycle of *Saccharomyces cerevisiae*. *J. Bacteriol.* **1984**, *158*, 701–704. [[CrossRef](#)]
16. Martínez-Salas, E.; Martín, J.A.; Vicente, M. Relationship of *Escherichia coli* density to growth rate and cell age. *J. Bacteriol.* **1981**, *147*, 97–100. [[CrossRef](#)] [[PubMed](#)]
17. Lin, L.; Choudhary, A.; Bavishi, A.; Ogbonna, N.; Maddux, S.; Choudhary, M. Use of the sucrose gradient method for bacterial cell cycle synchronization. *J. Microbiol. Biol. Educ.* **2012**, *13*, 50–53. [[CrossRef](#)]
18. Schrader, J.M.; Shapiro, L. Synchronization of *Caulobacter crescentus* for investigation of the bacterial cell cycle. *J. Vis. Exp.* **2015**, *98*, e52633. [[CrossRef](#)]
19. Wilmaerts, D.; Ethel, M.W.; Verstraeten, N.; Michiels, A.J. General Mechanisms Leading to Persister Formation and Awakening. *Trends Genet.* **2019**, *35*, 401–411. [[CrossRef](#)]
20. Kim, J.S.; Chowdhury, N.; Yamasaki, R.; Wood, T.K. Viable but non-culturable and persistence describe the same bacterial stress state. *Env. Microbiol.* **2018**, *20*, 2038–2048. [[CrossRef](#)]
21. Johnson, M.E.; Montoro Bustos, A.R.; Winchester, M.R. Practical utilization of spICP-MS to study sucrose density gradient centrifugation for the separation of nanoparticles. *Anal. Bioanal. Chem.* **2016**, *408*, 7629–7640. [[CrossRef](#)] [[PubMed](#)]
22. Chandra, K.; Kumar, V.; Werner, S.E.; Odom, T.W. Separation of Stabilized MOPS Gold Nanostars by Density Gradient Centrifugation. *ACS Omega* **2017**, *2*, 4878–4884. [[CrossRef](#)] [[PubMed](#)]
23. Sánchez-López, V.; Fernández-Romero, J.M.; Gómez-Hens, A. Evaluation of liposome populations using a sucrose density gradient centrifugation approach coupled to a continuous flow system. *Anal. Chim. Acta* **2009**, *645*, 79–85. [[CrossRef](#)] [[PubMed](#)]
24. Graham, J.M. Isolation of Golgi membranes from tissues and cells by differential and density gradient centrifugation. *Curr. Protoc. Cell Biol.* **2001**, *3.9*, 1–24. [[CrossRef](#)] [[PubMed](#)]
25. Hadjiolov, A.A.; Venkov, P.V.; Tsanev, R.G. Ribonucleic acids fractionation by density-gradient centrifugation and by agar gel electrophoresis: A comparison. *Anal. Biochem.* **1966**, *17*, 263–267. [[CrossRef](#)] [[PubMed](#)]
26. Zwartouw, H.T.; Westwood, J.C.; Appleyard, G. Purification of pox viruses by density gradient centrifugation. *J. Gen. Microbiol.* **1962**, *29*, 523–529. [[CrossRef](#)] [[PubMed](#)]
27. Brakke, M.K. Nonideal sedimentation and the capacity of sucrose gradient columns for virus in density-gradient centrifugation. *Arch. Biochem. Biophys.* **1964**, *107*, 388–403. [[CrossRef](#)]

28. Parlet, C.P.; Brown, M.M.; Horswill, A.R. Commensal *Staphylococci* Influence *Staphylococcus aureus* Skin Colonization and Disease. *Trends Microbiol.* **2019**, *27*, 497–507. [[CrossRef](#)] [[PubMed](#)]
29. Filkins, L.M.; Graber, J.A.; Olson, D.G.; Dolben, E.L.; Lynd, L.R.; Bhuju, S.; O'Toole, G.A. Coculture of *Staphylococcus aureus* with *Pseudomonas aeruginosa* Drives *S. aureus* towards Fermentative Metabolism and Reduced Viability in a Cystic Fibrosis Model. *J. Bacteriol.* **2015**, *197*, 2252–2264. [[CrossRef](#)]
30. Ciupescu, L.M.; Auvray, F.; Nicorescu, I.M.; Meheut, T.; Ciupescu, V.; Lardeux, A.L.; Tanasuica, R.; Hennekinne, J.A. Characterization of *Staphylococcus aureus* strains and evidence for the involvement of non-classical enterotoxin genes in food poisoning outbreaks. *FEMS Microbiol. Lett.* **2018**, *365*, fny139. [[CrossRef](#)]
31. Pollitt, E.J.; Crusz, S.A.; Diggle, S.P. *Staphylococcus aureus* forms spreading dendrites that have characteristics of active motility. *Sci. Rep.* **2015**, *5*, 17698. [[CrossRef](#)] [[PubMed](#)]
32. Cartwright, J.H.E. Stokes' law, viscometry, and the Stokes falling sphere clock. *Philos. Trans. A Math. Phys. Eng. Sci.* **2020**, *378*, 20200214. [[CrossRef](#)] [[PubMed](#)]
33. Gu, H.; Lee, S.W.; Carnicelli, J.; Jiang, Z.; Ren, D. Antibiotic Susceptibility of *Escherichia coli* Cells during Early-Stage Biofilm Formation. *J. Bacteriol.* **2019**, *201*, e00034-19. [[CrossRef](#)]
34. Naghili, H.; Tajik, H.; Mardani, K.; Razavi Rouhani, S.M.; Ehsani, A.; Zare, P. Validation of drop plate technique for bacterial enumeration by parametric and nonparametric tests. *Vet. Res. Forum* **2013**, *4*, 179–183.
35. O'Toole, G.A. Microtiter dish biofilm formation assay. *J. Vis. Exp.* **2011**, *47*, e2437. [[CrossRef](#)]
36. Schichnes, D.; Nemson, J.A.; Ruzin, S.E. Fluorescent Staining Method for Bacterial Endospores. *Microscope* **2006**, *54*, 91–93.
37. Sutton, S. The Most Probable Number Method and Its Uses in Enumeration, Qualification, and Validation. *J. Valid. Technol.* **2010**, *16*, 35–38.
38. Idrees, M.; Sawant, S.; Karodia, N.; Rahman, A. Biofilm: Morphology, Genetics, Pathogenesis and Treatment Strategies. *Int. J. Env. Res. Public Health* **2021**, *18*, 7602. [[CrossRef](#)]
39. Hindy, J.R.; Haddad, S.F.; Kanj, S.S. New drugs for methicillin-resistant *Staphylococcus aureus* skin and soft tissue infections. *Curr. Opin. Infect. Dis.* **2022**, *35*, 112–119. [[CrossRef](#)]
40. Arciola, C.R.; Campoccia, D.; Montanaro, L. Implant infections: Adhesion, biofilm formation and immune evasion. *Nat. Rev. Microbiol.* **2018**, *16*, 397–409. [[CrossRef](#)]
41. Mah, T.F.; O'Toole, G.A. Mechanisms of Biofilm Resistance to Antimicrobial Agents. *Trends Microbiol.* **2001**, *9*, 34–39. [[CrossRef](#)]
42. Stewart, P.S. Mechanisms of antibiotic resistance in bacterial biofilms. *Int. J. Med. Microbiol.* **2002**, *292*, 107–113. [[CrossRef](#)] [[PubMed](#)]
43. Mahto, K.U.; Das, S. Bacterial biofilm and extracellular polymeric substances in the moving bed biofilm reactor for wastewater treatment: A review. *Bioresour. Technol.* **2022**, *345*, 126476. [[CrossRef](#)] [[PubMed](#)]
44. Muhammad, M.H.; Idris, A.L.; Fan, X.; Guo, Y.; Yu, Y.; Jin, X.; Qiu, J.; Guan, X.; Huang, T. Beyond Risk: Bacterial Biofilms and Their Regulating Approaches. *Front. Microbiol.* **2020**, *11*, 928. [[CrossRef](#)] [[PubMed](#)]
45. Xu, Y.; Ren, D. A novel inductively coupled capacitor wireless sensor system for rapid antibiotic susceptibility testing. *J. Biol. Eng.* **2023**, *17*, 54. [[CrossRef](#)]
46. Gu, H.; Lee, S.W.; Carnicelli, J.; Zhang, T.; Ren, D. Magnetically driven active topography for long-term biofilm control. *Nat. Commun.* **2020**, *11*, 2211. [[CrossRef](#)] [[PubMed](#)]
47. Gu, H.; Lee, S.W.; Buffington, S.L.; Henderson, J.H.; Ren, D. On-Demand Removal of Bacterial Biofilms via Shape Memory Activation. *ACS Appl. Mater. Interfaces* **2016**, *8*, 21140–21144. [[CrossRef](#)]
48. Johnson, M.E.; Bustos, A.R.M.; Hanna, S.K.; Petersen, E.J.; Murphy, K.E.; Yu, L.L.; Nelson, B.C.; Winchester, M.R. Sucrose density gradient centrifugation for efficient separation of engineered nanoparticles from a model organism, *Caenorhabditis elegans*. NIST Special Publication 1200-24. *Natl. Inst. Stand. Technol.* **2017**. [[CrossRef](#)]
49. Damas-Souza, D.M.; Nunes, R.; Carvalho, H.F. An improved acridine orange staining of DNA/RNA. *Acta Histochem.* **2019**, *121*, 450–454. [[CrossRef](#)]
50. Lee, S.W.; Gu, H.; Kilberg, J.B.; Ren, D. Sensitizing bacterial cells to antibiotics by shape recovery triggered biofilm dispersion. *Acta Biomater.* **2018**, *81*, 93–102. [[CrossRef](#)]

Disclaimer/Publisher's Note: The statements, opinions and data contained in all publications are solely those of the individual author(s) and contributor(s) and not of MDPI and/or the editor(s). MDPI and/or the editor(s) disclaim responsibility for any injury to people or property resulting from any ideas, methods, instructions or products referred to in the content.